Epithelial NF-κB activation promotes urethane-induced lung carcinogenesis

Georgios T. Stathopoulos*†, Taylor P. Sherrill*‡, Dong-Sheng Cheng*, Robert M. Scoggins*, Wei Han*, Vasiliy V. Polosukhin*, Linda Connelly§, Fiona E. Yull§, Barbara Fingleton§, and Timothy S. Blackwell*‡§¶

*Department of Medicine, Division of Allergy, Pulmonary, and Critical Care, ‡Department of Cell and Developmental Biology, and §Department of Cancer Biology, Vanderbilt University School of Medicine, Nashville, TN 37232; and ¶Department of Veterans Affairs, Tennessee Valley Healthcare System, Nashville, TN 37212-2637

Edited by Inder M. Verma, Salk Institute for Biological Studies, La Jolla, CA, and approved September 21, 2007 (received for review June 6, 2007)

Chronic inflammation is linked to carcinogenesis in several organ systems. In the lungs, NF-κB, a central effector of inflammatory responses, is frequently activated in non-small-cell lung cancer, but its role in tumor promotion has not been studied. Several lines of evidence indicate that ethyl carbamate (urethane)-induced lung tumor formation, a prototypical mouse model of multistage lung carcinogenesis, is potentiated by inflammation. We found that mouse strains susceptible to lung tumor formation (FVB, BALB/c) exhibited early NF-κB activation and inflammation in the lungs after urethane treatment. However, a resistant strain (C57B6) failed to activate NF-κB or induce lung inflammation. In FVB mice, we identified urethane-induced NF-κB activation in airway epithelium, as well as type II alveolar epithelial cells and macrophages. Using an inducible transgenic mouse model (FVB strain) to express a dominant inhibitor of NF-κB specifically in airway epithelial cells, we found that urethane-induced lung inflammation was blocked and tumor formation was reduced by >50%. Selective NF-κB inhibition resulted in increased apoptosis of airway epithelial cells at 2 weeks after urethane treatment in association with a marked reduction of Bcl-2 expression. These studies indicate that NF-κB signaling in airway epithelium is integral to tumorigenesis in the urethane model and identify the NF-κB pathway as a potential target for chemoprevention of lung cancer.

apoptosis | cancer | inflammation | airway | adenocarcinoma

An epidemiological association between chronic inflammation and cancer has been recognized in several organ systems (1–3). In the lungs, this relationship is likely manifested by the association between chronic obstructive pulmonary disease (COPD) and the development of lung cancer. COPD represents a spectrum of pathophysiological alterations in the lungs, including chronic bronchitis and emphysema. However, a common feature of COPD is airway inflammation with infiltration of neutrophils, activated macrophages, and lymphocytes (4, 5). Several studies have confirmed that the development of COPD is an independent risk factor for lung cancer even when adjusted for age, sex, and smoking history (adjusted relative risk 2–5) (6–10).

The pathways connecting inflammation and tumor formation in the lungs have not been well characterized. However, NF-κB has been identified as an important promoter of tumorigenesis in some models of adenocarcinoma (AC) in the gastrointestinal tract (11, 12). NF-κB serves as a key regulatory pathway for the production of proinflammatory cytokines and chemokines, cell-cycle proteins, antiapoptotic proteins, and growth factors (13–15). The predominant mechanism of NF-κB activation involves phosphorylation, ubiquitination, and degradation of inhibitors of NF-κB (IκB), allowing NF-κB dimers to translocate to the nucleus and promote transcription of target genes (13–15). Activation of NF-κB is implicated in the pathogenesis of inflammatory disorders of the lungs, including COPD (16–18). In this regard, COPD patients have increased activation of NF-κB in lung macrophages and epithelial cells (16, 17). In addition, cigarette smoke induces NF-κB activation *in vivo* and *in vitro* (19, 20). Therefore, the NF-κB pathway is positioned to impact carcinogenesis in the lungs.

Treatment of mice with chemical carcinogens, including ethyl carbamate (urethane), has been used extensively to model multistage human lung carcinogenesis (21). Mouse lung tumors are thought to arise from nonciliated airway epithelial (Clara) or type II alveolar epithelial cells, and gene mutations described in mouse lung tumor cells are similar to those identified in human lung cancers (22, 23). Also, several studies have identified similarities in gene expression profiles between mouse lung tumors induced by chemical carcinogens and human ACs, further supporting the utility of these models (21, 23–25).

In these studies, we hypothesized that the NF-κB pathway regulates inflammation and tumorigenesis in the lungs after exposure to chemical carcinogens. We investigated whether activation of NF-κB and the development of inflammation correlate with tumor formation in the lungs from three inbred strains of mice expected to display different sensitivities to chemical carcinogenesis. We then identified NF-κB activation in airway epithelial cells after urethane treatment in a susceptible mouse strain and used an inducible transgenic mouse model (26) to selectively inhibit NF-κB in these cells. Together these studies identify a key role for NF-κB in promoting lung tumorigenesis.

Results

To determine whether activation of NF-κB in the lungs is associated with lung tumorigenesis after urethane treatment, we crossed NF-κB reporter mice [HIV-LTR.Luciferase (*HLL*)] expressing *Photinus pyralis* luciferase cDNA under control of the proximal 5′ HIV-LTR (27, 28) into the C57B6, BALB/c, and FVB backgrounds (more than nine generations). Existing data regarding strain-specific responses to urethane indicate that BALB/c and FVB mice are susceptible to lung tumor formation, whereas C57B6 are resistant (29). Mice in these studies received weekly i.p. injections of 1 g/kg urethane for 4 weeks and were imaged for bioluminescence (after luciferin injection) to detect NF-κB-dependent luciferase activity over the lungs at baseline (just before the first urethane dose) and 1, 2, and 3 weeks (before subsequent urethane dosing) (Fig. 1*A*). Quantification of bioluminescence over the chest (n = 6–8 per strain) showed that

Author contributions: G.T.S., F.E.Y., B.F., and T.S.B. designed research; G.T.S., T.P.S., D.-S.C., R.M.S., W.H., V.V.P., L.C., and B.F. performed research; D.-S.C., F.E.Y., B.F., and T.S.B. contributed new reagents/analytic tools; G.T.S., F.E.Y., B.F., and T.S.B. analyzed data; and G.T.S., F.E.Y., B.F., and T.S.B. wrote the paper.

The authors declare no conflict of interest.

This article is a PNAS Direct Submission.

Abbreviations: IκB, inhibitor of NF-κB; IKK, IκB kinase; COPD, chronic obstructive pulmonary disease; CT, computerized tomography; AAH, atypical adenomatous hyperplasia; AD, adenoma; AC, adenocarcinoma; BAL, bronchoalveolar lavage; dox, doxycycline; DNTA, IκBα-DN trans-activated.

†To whom correspondence should be addressed. E-mail: gstathop@med.uoa.gr.

This article contains supporting information online at www.pnas.org/cgi/content/full/0705316104/DC1.

© 2007 by The National Academy of Sciences of the USA

Downloaded from https://www.pnas.org by 18.97.9.173 on April 21, 2025 from IP address 18.97.9.173.

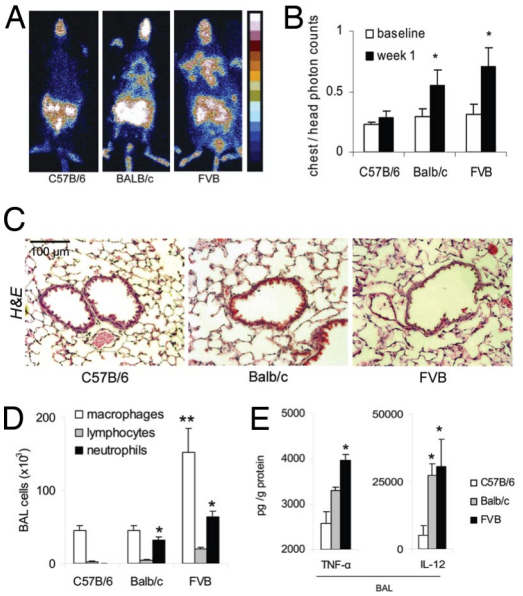

Fig. 1. Mouse-strain-dependent NF-κB activation and lung inflammation at 1 week after i.p. injection of 1 g/kg urethane. (*A*) Representative bioluminescence images of NF-κB reporter mice (*HLL*) from different strains showing NF-κB-dependent luciferase activity at 1 week after urethane. (*B*) Bar graph showing lung bioluminescence in *HLL* mice (normalized to head bioluminescence to correct for strain-related baseline differences) ($n = 6–8$ per group; *, $P < 0.05$ compared with baseline). (*C*) Representative lung tissue sections stained with H&E. (*D*) Differential cell counts in BAL ($n = 4$ per group; *, $P < 0.01$ compared with C57B6; **, $P < 0.01$ compared with other strains). (*E*) TNF-α and IL-12p70 levels in BAL fluid ($n = 4$ per group; *, $P < 0.05$ compared with C57B6).

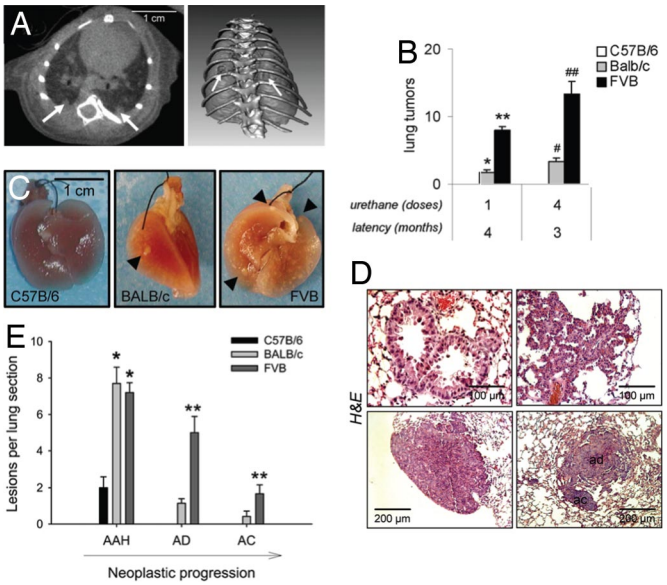

Fig. 2. Strain-dependent susceptibility to urethane-induced lung tumorigenesis. C57B6, BALB/c, and FVB mice received i.p. injections of 1 g/kg urethane in two protocols: four weekly injections with 3-month latency until harvest or a single injection with 4-month latency. (*A*) MicroCT images of FVB mouse 3 months after initiation of multidose urethane protocol showing lung tumors (arrows). (*B*) Mean lung tumor number in mice treated according to the two protocols ($n = 9–36$ per group; $P < 0.001$ compared with: * and #, C57B6; ** and ##, C57B6 and BALB/c). (*C*) Representative photographs of lungs 3 months after multidose urethane. (*D*) Representative photomicrographs of lungs 3 months after multidose urethane showing Clara cell hyperplasia (*Upper Left*), AAH (*Upper Right*), AD (*Lower Left*), and AD with a focus of AC (*Lower Right*). (*E*) Number of neoplastic lesions (AAH, AD, and AC) per lung section in mice 3 months after multidose urethane ($n = 6$ per group; *, $P < 0.001$ compared with C57B6; **, $P < 0.01$ compared with BALB/c and C57B6).

luciferase activity was induced in BALB/c and FVB *HLL* mice, but not in C57B6 *HLL* mice (Fig. 1*B*). Increased bioluminescence after urethane treatment was not detected over other regions (i.e., abdomen, head). By week 3, chest bioluminescence returned toward baseline (data not shown). These results indicated that urethane-induced activation of NF-κB occurs in the lungs of BALB/c *HLL* and FVB *HLL*, but not C57B6 *HLL*, mice.

Once we identified NF-κB activation after urethane treatment, we assessed whether this finding was correlated with lung inflammation. For these studies, WT mice from the aforementioned strains ($n = 10$ per strain) received a single i.p. injection of 1 g/kg urethane, and lungs were harvested 1 week later for evaluation of histology ($n = 6$ per strain) and for inflammatory cells and cytokines in bronchoalveolar lavage (BAL) fluid ($n = 4$ per strain). One week after urethane, FVB mice exhibited a predominantly interstitial inflammatory lung infiltrate (primarily neutrophils and monocytes/macrophages), BALB/c mice an intermediate phenotype, and C57B6 mice no histological evidence of inflammation (Fig. 1*C*). Compared with C57B6 mice, FVB and BALB/c mice also had increased inflammatory cells in BAL (Fig. 1*D*). Total and differential BAL cell counts from untreated C57B6, BALB/c, and FVB mice were similar to urethane-treated C57B6 mice (data not shown). In addition, FVB and BALB/c mice had increased circulating neutrophils compared with C57B6 mice (3.5 ± 0.5, 2.1 ± 0.5, and $0.7 \pm 0.2 \times 10^3/\mu$l, respectively; $P < .05$), whereas no differences were found in other WBC lineages (data not shown). We next determined the levels of inflammatory mediators (IL-6, IL-10, IL-12p70, TNF-α, IFN-γ, and MCP-1) in BAL fluid by using a cytometric bead array. One week after urethane, FVB and BALB/c mice showed increased TNF-α and IL-12p70 levels compared with C57B6 mice (Fig. 1*E*). No differences were found for IL-6, IL-10, IFN-γ, or MCP-1. However, concentrations of these cytokines were not increased significantly in urethane-treated mice compared with untreated controls. Collectively, these results indicate that urethane-induced NF-κB activation is associated with the development of lung inflammation.

To correlate early lung inflammation and NF-κB activation in different mouse strains with subsequent tumor formation in the multidose urethane model, we screened mice from each strain by micro-computerized tomography (CT) for lung tumor appearance starting at 2 months after urethane initiation. Lung tumors were detected in FVB mice 3 months after starting urethane (Fig. 2*A*), at which time animals were killed. Urethane-induced tumors were visible on the lung surface of FVB and BALB/c, but not C57B6, mice (Fig. 2 *B* and *C*). We also performed experiments by using a single i.p. injection of urethane and killed mice at 4 months when tumors were identified by microCT. Again, lung tumors were present in FVB and BALB/c, but not C75B6, mice (Fig. 2*B*). We performed an extensive histological evaluation of lungs from C57B6, BALB/c, and FVB mice treated with multidose urethane and found a range of neoplastic lesions: atypical adenomatous hyperplasia (AAH), papillary and solid adenoma (AD), and AC (Fig. 2*D*). All types of lesions were identified in lungs from FVB and BALB/c mice, although FVB mice had greater numbers of AD and AC than BALB/c mice (Fig. 2*E*). In contrast, lungs from C57B6 mice had areas of AAH, but no progression to AD or AC occurred. Enumeration of lung tumors on transverse lung sections correlated well with macroscopic lung tumor counting ($n = 21$, $\rho = 0.971$, $P = 10^{-6}$), validating the latter as a tumor quantification approach as described previously (30). Tumor formation was only observed in strains of mice with early NF-κB activation and inflammation in the lungs after urethane treatment.

To define the timing, dose-response, and cellular distribution of urethane-induced NF-κB activation in the lungs of susceptible mice, we used another NF-κB reporter mouse model [NF-κB.GFP.Lu-

Downloaded from https://www.pnas.org by 18.97.9.173 on April 21, 2025 from IP address 18.97.9.173.

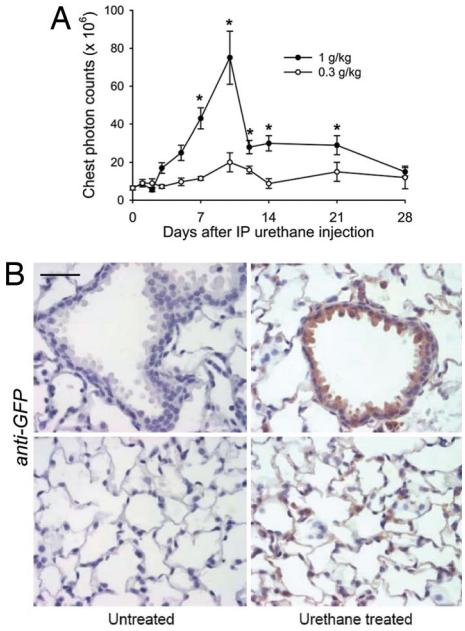

Fig. 3. Characterization of lung NF-κB activation in response to urethane. NF-κB reporter (*NGL*) mice (FVB strain) received 0.3 or 1 g/kg urethane by i.p. injection. (*A*) Time course of NF-κB-dependent lung bioluminescence ($n = 3$ per group; *, $P < 0.05$ compared with baseline). (*B*) GFP immunostaining in lung tissue from *NGL* reporter mice. (*Left*) Untreated. (*Right*) Ten days after 1 g/kg urethane. GFP staining (brown) identifies NF-κB activation in airway epithelium, alveolar type II cells, and macrophages. (Scale bar: 50 μm.)

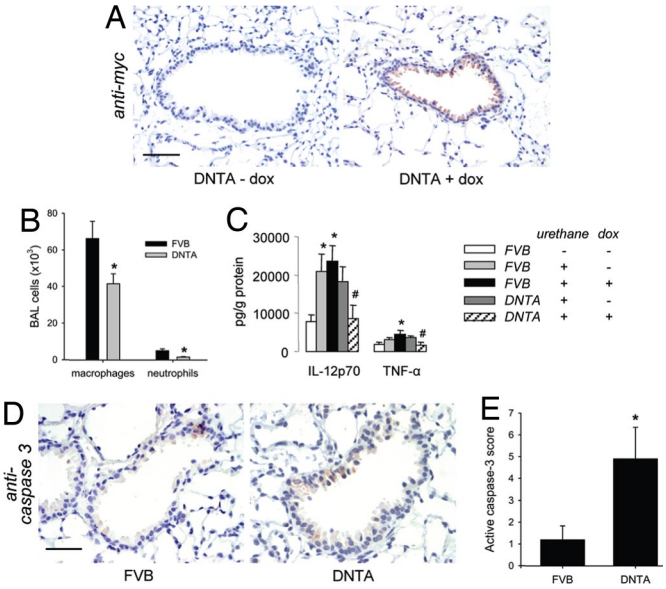

Fig. 4. Inhibition of NF-κB in airway epithelium reduces urethane-induced inflammation and increases epithelial apoptosis. (*A*) Lung tissue sections from DNTA transgenic mice with or without dox treatment (1 g/liter in their drinking water) for 1 week were immunostained with anti-Myc Abs to identify expression of the transgene (myc-tagged IκBα-DN). Transgene expression is limited to airway epithelium. (Scale bar: 50 μm.) (*B*) FVB control and DNTA mice were treated with dox in their drinking water for 1 week, followed by i.p. injection of 1 g/kg urethane and harvested 2 weeks later with continued dox treatment. Differential cell counts in BAL (FVB, $n = 6$; DNTA, $n = 9$; *, $P < 0.05$ compared with FVB). (*C*) Similar experiment in which FVB controls and DNTA mice were treated with or without dox and with or without urethane and harvested at 1 week after urethane. Cytokines were measured in BAL fluid ($n = 5$ per group; *, $P < 0.05$ compared with FVB without urethane and dox; #, $P < 0.05$ compared with FVB plus urethane with or without dox). (*D*) Representative lung sections immunostained (brown) for active caspase-3 at 2 weeks after turethane in the experiment described in *B*. (Scale bar: 50 μm.) (*E*) Scoring of active caspase-3 staining in airway epithelium (FVB, $n = 6$; DNTA, $n = 9$; *, $P < 0.05$ compared with FVB).

ciferase (*NGL*)], in which a synthetic NF-κB promoter drives the expression of a GFP-luciferase fusion protein (31). *NGL* mice (FVB background) were treated with a single i.p. injection of 0.3–3 g/kg urethane, and serial bioluminescence imaging was performed (Fig. 3*A*). The 3 g/kg dose resulted in death by 24 h, but all mice treated with 0.3 and 1 g/kg survived. Chest bioluminescence peaked at day 10 after urethane in the 1 g/kg group and returned toward baseline by 4 weeks. No significant increase in bioluminescence was noted in the 0.3 g/kg group. In separate experiments, lungs from *NGL* mice were harvested 10 days after urethane, and GFP expression was identified by immunohistochemistry. GFP expression was minimal in lung sections from untreated *NGL* mice, whereas significant GFP expression was detected in the lungs from urethane-treated *NGL* mice. NF-κB-dependent GFP expression was identified in airway epithelium, type II alveolar epithelial cells, and macrophages (Fig. 3*B*).

Based on the identification of NF-κB activation in airway epithelial cells of a mouse strain susceptible to urethane, we undertook experiments to block NF-κB signaling in these cells and to determine the impact on urethane-induced lung inflammation and tumor formation. We used inducible transgenic mice on the urethane-susceptible FVB background that selectively express a dominant inhibitor of NF-κB (IκBα-DN) under the control of the Clara cell-specific CC10 promoter (26, 32–34). After addition of doxycycline (dox) to drinking water, expression of IκBα-DN in the lungs of these transgenic [IκBα-DN trans-activated (DNTA)] mice has been shown to block NF-κB activation in response to inflammatory stimuli (26). To verify selective transgene expression in airway epithelium in this model, DNTA mice were given 1 g/liter dox in their drinking water for 1 week, and expression of the Myc-tagged transgene was assessed in lung tissue (Fig. 4*A*) and BAL cells (data not shown). Transgene expression was strictly confined to airway lining epithelium and was not evident in other cell types in lung tissue or BAL. Next, DNTA mice (and nontransgenic FVB littermates) were treated with a single i.p. injection of urethane, and lungs were harvested up to 2 weeks later to determine whether blocking NF-κB in airway epithelium could impact lung inflammation and/or epithelial cell survival after urethane. To assess lung inflammation, inflammatory cells and cytokines were measured in BAL. Macrophages and neutrophils were reduced in BAL from urethane-treated DNTA mice, compared with FVB controls (both treated with dox) (Fig. 4*B*). In addition, IL-12p70 and TNF-α levels in BAL fluid were reduced in dox- and urethane-treated DNTA mice compared with controls (Fig. 4*C*). These results indicate that NF-κB signaling in airway epithelium contributes to urethane-induced lung inflammation.

In addition to inflammation, NF-κB can impact cell survival through the induction of antiapoptotic genes. Therefore, we performed immunostaining for active caspase-3 and TUNEL on lung sections harvested at 2 weeks after urethane as markers for apoptosis. Significantly more active caspase-3 (Fig. 4 *D* and *E*) and TUNEL (data not shown) staining was identified in airway epithelium of DNTA mice compared with controls. Because several antiapoptotic proteins, including Bcl-2, Bcl-x_L, cIAP-1, and XIAP, are regulated by the NF-κB pathway (35, 36), we evaluated lungs for differences in the expression of these proteins by Western blot. As shown in Fig. 5 *A* and *B*, Bcl-2 expression was reduced in DNTA mouse lungs at 2 weeks after urethane, but no differences were observed for the other proteins. Subsequently, we performed immunohistochemistry for Bcl-2 expression to show that the reduction of Bcl-2 was localized to airway epithelium (Fig. 5 *C* and *D*).

Downloaded from https://www.pnas.org by 18.97.9.173 on April 21, 2025 from IP address 18.97.9.173.

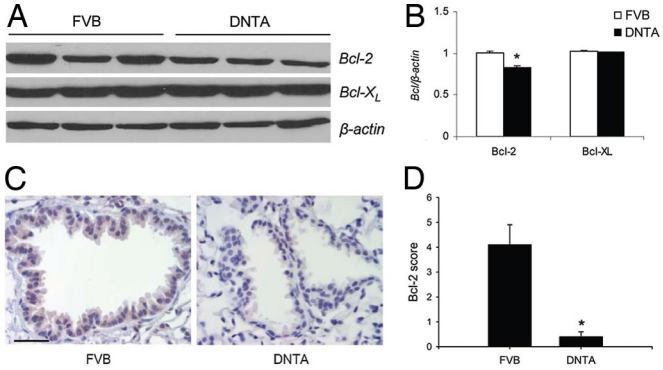

Fig. 5. Reduced urethane-induced Bcl-2 expression in lungs of DNTA mice. FVB control and DNTA mice were treated with dox in their drinking water for 1 week, followed by i.p. injection of 1 g/kg urethane and harvested 2 weeks later with continued dox treatment. (*A*) Western blots for Bcl-2 and Bcl-X_L in whole-lung tissue. (*B*) Densitometry data obtained from bands on Western blots normalized for β-actin (FVB, $n = 8$; DNTA, $n = 11$; *, $P < 0.05$ compared with FVB). (*C*) Immunostaining for Bcl-2 (brown) in airway from FVB (*Left*) and DNTA mouse (*Right*). (Scale bar: 50 μm.) (*D*) Scoring of lung sections for Bcl-2 expression in airway epithelial cells (FVB, $n = 6$; DNTA, $n = 9$; *, $P < 0.05$).

These data suggested that NF-κB activation is required for Bcl-2 expression in the airways after urethane treatment.

To determine whether alterations in urethane-induced lung inflammation and apoptosis translated into differences in tumor formation, DTNA mice and FVB controls were treated with dox for 1 week, followed by a single i.p. injection of 1 g/kg urethane. Dox was continued throughout the experiment in both groups, and lungs were harvested at 4 months after urethane injection. DNTA mice developed 58% fewer lung surface tumors than FVB controls (Fig. 6*A*). No difference in mean tumor size or histological appearance of tumors was identified (Fig. 6 *B* and *C*). On lung sections, no ACs were found in either group, but AAH lesions and adenomas were markedly reduced in DNTA mice (Fig. 6*D*). At the time of harvest, lung inflammation was not prominent in either group. BAL total cell counts were similar between the groups, and ≥97% of cells were macrophages in both groups. In addition, no differences between groups were detected in BAL cytokines, peripheral WBC counts, and differentials.

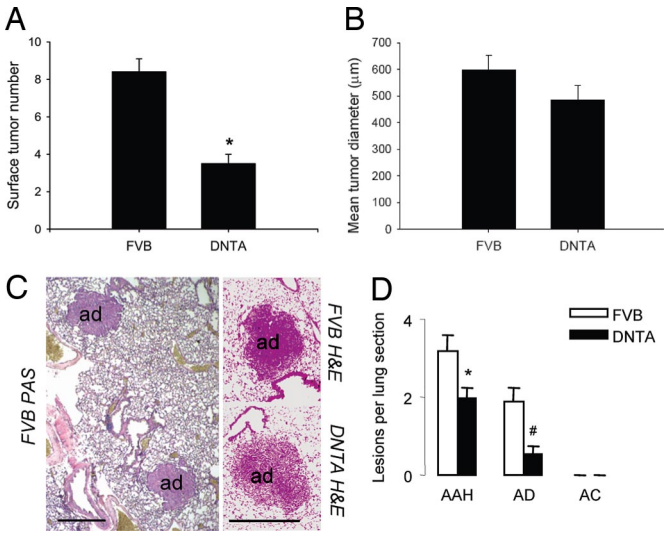

Fig. 6. Reduction of lung tumor formation in DNTA mice. FVB control and DNTA mice were treated with dox in their drinking water for 1 week, followed by i.p. injection of 1 g/kg urethane, and lungs were harvested 4 months later with continued dox treatment. (*A*) Average lung surface tumor number per mouse (FVB, $n = 22$; DNTA, $n = 11$; *, $P < 0.001$ compared with FVB). (*B*) Average lung tumor diameter per mouse on H&E-stained lung sections (FVB, $n = 15$; DNTA, $n = 10$; $P > 0.05$). (*C*) Representative photomicrographs of lung tumors stained with periodic acid/ Schiff (PAS) reagent showing mucin production (*Left*) and H&E (*Right*). (Scale bars: 500 μm.) (*D*) Number of neoplastic lesions per lung section (FVB, $n = 15$; DNTA, $n = 10$; *, $P = 0.04$; #, $P = 0.007$ compared with FVB).

Discussion

In these studies, we identified a tumor-promoting role for NF-κB in airway epithelium. We found that the susceptibility of different mouse strains to urethane-induced lung tumorigenesis correlates with the development of lung inflammation and NF-κB activation in airway epithelium at early time points. We then used transgenic mice from a susceptible strain that conditionally express a dominant inhibitor of NF-κB exclusively in airway epithelial cells to show that blocking NF-κB in these cells reduces carcinogenesis by >50%. Epithelial NF-κB activation is required for both lung inflammation and epithelial cell survival after urethane treatment, and the impact of NF-κB on epithelial survival is likely mediated through the induction of antiapoptotic mediators, including Bcl-2. These studies identify airway epithelial NF-κB signaling as an integral component of urethane-induced tumorigenesis.

Several lines of evidence support the idea that lung inflammation enhances experimental chemical lung tumorigenesis. First, butylated hydroxytoluene functions as a lung tumor promoter only in mouse strains in which it produces lung inflammation (37). Second, TNF-α and IL-10 haploinsufficient mice display altered susceptibility to chemical-induced lung tumor formation (30). Third, genes responsible for the lung inflammatory response cosegregate with genes conferring susceptibility to chemical lung tumorigenesis within pulmonary adenoma susceptibility genetic loci (38), and the murine TNF-α gene has been identified as a strong candidate within the pulmonary adenoma susceptibility-2 locus (39, 40). In our studies, inflammatory cell influx, increased TNF-α and/or IL-12p70 production, and activation of NF-κB were identified in the lungs of mouse strains susceptible to urethane tumorigenesis (FVB and BALB/c), but not of a resistant strain (C57B6). These findings strengthen the connection between inflammatory pathways and lung carcinogenesis in experimental models.

In the lungs, NF-κB is activated by many noxious/inflammatory/infectious stimuli, implicating the NF-κB pathway as a focal point for innate immune responses. In addition, NF-κB is activated by a number of carcinogens and induces proteins that enhance cell survival/proliferation (13–15). In cells and animal models, cigarette smoke induces NF-κB activation (19, 20). NF-κB is activated in some lung cancer cell lines and renders them resistant to chemotherapy (41, 42). In addition, NF-κB is frequently activated in lung cancer specimens obtained by resection or biopsy (43, 44). A recent study identified high levels of nuclear RelA (an indicator of NF-κB activation) in non-small-cell lung cancers and AAH compared with normal epithelium (44). Although previous studies have highlighted an association between NF-κB and human lung cancer, our data provide experimental evidence that the NF-κB pathway can directly promote lung tumor formation. This interface between NF-κB signaling and the development of lung cancer may be particularly important in patients with chronic airway inflammation, including COPD.

Although the impact of NF-κB on lung carcinogenesis has not been previously investigated in animal models, studies using conditional loss of function approaches to investigate NF-κB signaling in cancer of the gastrointestinal tract have had mixed results. In one study, mice in which IκB kinase 2 (IKK2) was conditionally eliminated in intestinal epithelial cells developed 75% fewer colon tumors after administration of azoxymethane and dextran sulfate (11). Controls exhibited induction of antiapoptotic Bcl-X_L, which did not occur in IKK2-deficient mice. In another study, NF-κB inhibition in hepatocytes was found to reduce the number and size

Downloaded from https://www.pnas.org by 18.97.9.173 on April 21, 2025 from IP address 18.97.9.173.

of hepatocellular carcinomas in a mouse model of spontaneous cholestatic hepatitis leading to hepatic cancer (*Mdr2*-KO) (12). In contrast, IKK2 deletion in hepatocytes enhanced chemical-induced carcinogenesis in the liver (45). Similarly, deletion of IKK-γ/NEMO, an essential component of the IKK complex, resulted in the blockade of NF-κB signaling in hepatocytes and spontaneous hepatocellular carcinogenesis (46). Although these findings indicate that NF-κB impacts carcinogenesis, its effects on tumor formation appear to be tissue- and cell type-specific.

In our studies, selective NF-κB inhibition in Clara cells resulted in a substantial reduction in lung tumorigenesis. Although our approach has the advantage of identifying the contribution of a specific and defined population of cells within the lung microenvironment, these studies may have underestimated the total impact of NF-κB signaling on lung tumor formation because NF-κB inhibition was limited to cells expressing the CC10 promoter. Urethane-induced NF-κB activation was found in type II alveolar epithelial cells and macrophages (as well as airway epithelium), and NF-κB signaling in these cells also could impact tumorigenesis through direct (cell-autonomous) or indirect (paracrine) effects. Although a more complete understanding of the role of NF-κB in lung tumor promotion is the subject of ongoing investigations, our finding that NF-κB inhibition in airway epithelium blocks urethane-induced Bcl-2 expression and increases apoptosis after urethane treatment suggests that NF-κB contributes to lung tumorigenesis by directly promoting the survival of mutated or initiated epithelial cells. This idea is supported by the finding that DNTA mice have fewer precursor (AAH) lesions and fewer adenomas than control mice.

Lung cancer is a contemporary pandemic causing more deaths per year in the United States than the next three leading cancers combined (47). Although smoking cessation is fundamental in halting the lung cancer epidemic, additional prevention strategies are desperately needed because many patients continue to smoke, and currently most lung cancers develop in ex-smokers (48, 49). Identifying molecular links between smoking-induced lung inflammation and lung cancer may have important implications for defining individual lung cancer risk and tailoring chemoprevention therapies. Using an established mouse model of multistage lung tumorigenesis, we found that NF-κB contributes to carcinogen-induced inflammation and subsequent lung tumor formation. Based on these and future studies, detecting specific NF-κB-regulated inflammatory mediators produced in the lungs may help stratify individual risk for lung cancer development, and targeting NF-κB activation and associated inflammation may prove to be an effective strategy to prevent lung cancer in high-risk individuals, including those with COPD.

Materials and Methods

Details are provided in supporting information (SI) *Materials and Methods*.

Animal Model. All animal experiments were approved by Institutional Animal Care and Use guidelines. Mice used for experiments were sex, weight, and age matched. Tumors were induced by i.p. injection of 1 g/kg urethane in two protocols: a single urethane injection and 4-month latency and four consecutive weekly urethane injections and 3-month latency.

To evaluate NF-κB activation after urethane treatment, we fully back-crossed (more than nine generations) transgenic *HLL* (27, 28) and *NGL* (31) reporter mice into the C57B6, BALB/c, and FVB strains. To inhibit NF-κB in airway epithelial cells, we used inducible transgenic mice based on the tet-on system (DNTA, FVB background) expressing a Myc-His-tagged mutant avian IκBα that cannot be degraded (26, 32–34). To achieve selective expression in airway epithelium, mice containing tet-O_7-IκBα-DN constructs were crossed to mice expressing reverse tetracycline transactivator under control of the rat CC10 promoter (26). Transgene expression was induced by addition of 1 g/liter dox (Sigma–Aldrich, St. Louis, MO) in 2% sucrose to drinking water. DNTA mice from two separate founder lines were used for these studies.

CT Scanning. MicroCT images were acquired on an ImTek microCAT II scanner (ImTek, Knoxville, TN) as described previously (50).

Bioluminescent Imaging. Mice received 1 mg of D-luciferin and were imaged in a C2400–32-intensified, charged-coupled device (Hamamatsu, Bridgewater, NJ). Data were collected and analyzed by using customized hardware and software. Standard-sized circular regions of interest encompassing the murine chest, abdomen, and head were determined, and photon counts were measured over these areas (27, 28, 31).

Lung Tumor Enumeration. Surface tumors were counted by three blinded readers under a dissecting microscope and averaged as previously described (30). Tumor diameter was determined by using microcalipers.

Histology and Immunohistochemistry. Lungs were fixed in 10% neutral buffered formalin, followed by 70% ethanol. Tissues were embedded in paraffin, and 5-μm-thick sections were cut at the median transverse level of the lungs. Sections were mounted on glass slides and stained with H&E. Neoplastic lesions were counted by three blinded readers and averaged. GFP, TUNEL, active caspase-3, and Bcl-2 immunostaining, as well as semiquantitative scoring of active caspase-3 and Bcl-2, were done as described previously (27, 51, 52).

Total and Differential Cell Counting. BAL was performed with 3 × 800 μl of normal saline, and the total cell count was determined by using a grid hemocytometer. Cell differentials were obtained by counting at least 200 cells on Wright-Giemsa-stained cytocentrifuge slides.

Cytokine Measurements. Proinflammatory mediators (IL-6, IL-10, IL-12p70, TNF-α, IFN-γ, and MCP-1) were determined in cell-free BAL by using a cytometric bead array (BD Biosciences, San Diego, CA) (53) after heat-free vacuum centrifugation-mediated condensation. Cytokine levels were corrected for BAL protein and determined by a bicinchonic acid assay (Pierce, Rockford, IL).

SDS/PAGE and Western Blot Analysis. Equal volumes of lung protein extracts were subjected to SDS/PAGE and Western blotting as previously described (52) by using anti-Bcl-2, anti-Bcl-x_L(Cell Signaling Technology, Danvers, MA), anti-actin, and HRP-conjugated anti-rabbit IgG (Santa Cruz Biotechnology, Santa Cruz, CA) Abs.

Statistical Analysis. All values given represent mean ± SEM. To compare means between groups, Student's *t* test or ANOVA with LSD post hoc tests were used. Spearman's correlation was used to detect significant associations between variables (correlation coefficient = ρ). All *P* values were two-tailed. *P* values < .05 were considered significant. Statistical analyses were performed by using the Statistical Package for the Social Sciences Software Version 11.0 (SPSS, Chicago, IL).

This work was supported by National Institutes of Health Grants HL66196 and HL61419, the Department of Veterans Affairs (T.S.B.), and the Greek State Scholarship Foundation (G.T.S.).

Downloaded from https://www.pnas.org by 18.97.9.173 on April 21, 2025 from IP address 18.97.9.173.

1. Coussens LM, Werb Z (2002) *Nature* 420:860–867.
2. Balkwill F, Coussens LM (2004) *Nature* 431:405–406.
3. Karin M, Lawrence T, Nizet V (2006) *Cell* 124:823–835.
4. American Thoracic Society (1995) *Am J Respir Crit Care Med* 152:S77–S121.
5. Pauwels RA, Buist AS, Calverley PM, Jenkins CR, Hurd SS, the GOLD Scientific Committee (2001) *Am J Respir Crit Care Med* 163:1256–1276.
6. Skillrud DM, Offord KP, Miller RD (1986) *Ann Intern Med* 105:503–507.
7. Tockman MS, Anthonisen NR, Wright EC, Donithan MG (1987) *Ann Intern Med* 106:512–518.
8. Kuller LH, Ockene J, Meilahn E, Svendsen KH (1990) *Am J Epidemiol* 132:265–274.
9. Nomura A, Stemmermann GN, Chyou PH, Marcus EB, Buist AS (1991) *Am Rev Respir Dis* 144:307–311.
10. Prindiville SA, Byers T, Hirsch FR, Franklin WA, Miller YE, Vu KO, Wolf HJ, Baron AE, Shroyer KR, Zeng C, *et al*. (2003) *Cancer Epidemiol Biomarkers Prev* 12:987–993.
11. Greten FR, Eckmann L, Greten TF, Park JM, Li ZW, Egan LJ, Kagnoff MF, Karin M (2004) *Cell* 118:285–296.
12. Pikarsky E, Porat RM, Stein I, Abramovitch R, Amit S, Kasem S, Gutkovich-Pyest E, Urieli-Shoval S, Galun E, Ben Neriah Y (2004) *Nature* 431:461–466.
13. Karin M, Yamamoto Y, Wang QM (2004) *Nat Rev Drug Discov* 3:17–26.
14. Garg A, Aggarwal BB (2002) *Leukemia* 1053–1068.
15. Zhang Y, Chen F (2004) *Cancer Res* 64:1902–1905.
16. Di Stefano A, Caramori G, Oates T, Capelli A, Lusuardi M, Gnemmi I, Ioli F, Chung KF, Donner CF, Barnes PJ, *et al*. (2002) *Eur Respir J* 20:556–563.
17. Caramori G, Romagnoli M, Casolari P, Bellettato C, Casoni G, Boschetto P, Chung KF, Barnes PJ, Adcock IM, Ciaccia A, *et al*. (2003) *Thorax* 58:348–351.
18. Inayama M, Nishioka Y, Azuma M, Muto S, Aono Y, Makino H, Tani K, Uehara H, Izumi K, Itai A, *et al*. (2006) *Am J Respir Crit Care Med* 173:1016–1022.
19. Anto RJ, Mukhopadhyay A, Shishodia S, Gairola CG, Aggarwal BB (2002) *Carcinogenesis* 23:1511–1518.
20. Shishodia S, Potdar P, Gairola CG, Aggarwal BB (2003) *Carcinogenesis* 24:1269–1279.
21. Tuveson DA, Jacks T (1999) *Oncogene* 18:5318–5324.
22. Malkinson AM (2001) *Lung Cancer* 32:265–279.
23. Malkinson AM (1998) *Exp Lung Res* 24:541–555.
24. Johnson L, Mercer K, Greenbaum D, Bronson RT, Crowley D, Tuveson DA, Jacks T (2001) *Nature* 410:1111–1116.
25. Dragani TA (2003) *Cancer Res* 63:3011–3018.
26. Cheng DS, Han W, Chen SM, Sherrill TP, Chont M, Park GY, Sheller JR, Polosukhin VV, Christman JW, Yull FE, *et al*. (2007) *J Immunol* 178:6504–6513.
27. Blackwell TS, Yull FE, Chen CL, Venkatakrishnan A, Blackwell TR, Hicks DJ, Lancaster LH, Christman JW, Kerr LD (2000) *Am J Respir Crit Care Med* 162:1095–1101.
28. Yull FE, Han W, Jansen ED, Everhart MB, Sadikot RT, Christman JW, Blackwell TS (2003) *J Histochem Cytochem* 51:741–749.
29. Malkinson AM (1989) *Toxicology* 54:241–271.
30. Bernert H, Sekikawa K, Radcliffe RA, Iraqi F, You M, Malkinson AM (2003) *Mol Carcinog* 38:117–123.
31. Everhart MB, Han W, Sherrill TP, Arutiunov M, Polosukhin VV, Burke JR, Sadikot RT, Christman JW, Yull FE, Blackwell TS (2006) *J Immunol* 176:4995–5005.
32. Gossen M, Bujard H (1992) *Proc Natl Acad Sci USA* 89:5547–5551.
33. Deuschle U, Meyer WK, Thiesen HJ (1995) *Mol Cell Biol* 15:1907–1914.
34. Forster K, Helbl V, Lederer T, Urlinger S, Wittenburg N, Hillen W (1999) *Nucleic Acids Res* 27:708–710.
35. Bharti AC, Aggarwal BB (2002) *Biochem Pharmacol* 64:883–888.
36. Karin M, Lin A (2002) *Nat Immunol* 3:221–227.
37. Malkinson AM, Bauer A, Meyer A, Dwyer-Nield L, Koski K, Keith R, Geraci M, Miller YE (2000) *Chest* 117:228S.
38. Maria DA, Manenti G, Galbiati F, Ribeiro OG, Cabrera WH, Barrera RG, Pettinicchio A, De Franco M, Starobinas N, Siqueira M, *et al*. (2003) *Oncogene* 22:426–432.
39. Festing MF, Yang A, Malkinson AM (1994) *Genet Res* 64:99–106.
40. Fijneman RJ, Oomen LC, Snoek M, Demant P (1995) *Immunogenetics* 41:106–109.
41. Batra RK, Guttridge DC, Brenner DA, Dubinett SM, Baldwin AS, Boucher RC (1999) *Am J Respir cell Mol Biol* 21:238–245.
42. Kim JY, Lee S, Hwangbo B, Lee CT, Kim YW, Han SK, Shim YS, Yoo CG (2000) *Biochem Biophys Res Commun* 273:140–146.
43. Tichelaar JW, Zhang Y, leRiche JC, Biddinger PW, Lam S, Anderson MW (2005) *BMC Cancer* 5:155.
44. Tang X, Liu D, Shishodia S, Ozburn N, Behrens C, Lee JJ, Hong WK, Aggarwal BB, Wistuba II (2006) *Cancer* 107:2637–2646.
45. Sakurai T, Maeda S, Chang L, Karin M (2006) *Proc Natl Acad Sci USA* 103:10544–10551.
46. Luedde T, Beraza N, Kotsikoris V, Van LG, Nenci A, De VR, Roskams T, Trautwein C, Pasparakis M (2007) *Cancer Cell* 11:119–132.
47. Jemal A, Siegel R, Ward E, Murray T, Xu J, Smigal C, Thun MJ (2006) *CA Cancer J Clin* 56:106–130.
48. Doll R, Peto R (1978) *J Epidemiol Commun Health* 32:303–313.
49. Peto R, Lopez AD, Boreham J, Thun M (2006) *Mortality from Smoking in Developed Countries 1950–2000* (Oxford Univ Press, Oxford, UK); freely available at www.ctsu.ox.ac.uk/~tobacco.
50. Stathopoulos GT, Zhu Z, Everhart MB, Kalomenidis I, Lawson WE, Bilaceroglu S, Peterson TE, Mitchell D, Yull FE, Light RW, *et al*. (2006) *Am J Respir Cell Mol Biol* 34:142–150.
51. Lawson WE, Polosukhin VV, Stathopoulos GT, Zoia O, Han W, Lane KB, Li B, Donnelly EF, Holburn GE, Lewis KG, *et al*. (2005) *Am J Pathol* 167:1267–1277.
52. Connelly L, Robinson-Benion C, Chont M, Saint-Jean L, Li H, Polosukhin VV, Blackwell TS, Yull FE (2007) *J Biol Chem* 282:10028–10035.
53. McHugh TM (1994) *Method Cell Biol* 42:575–595.

Downloaded from https://www.pnas.org by 18.97.9.173 on April 21, 2025 from IP address 18.97.9.173.